Journal of Zhejiang University-SCIENCE A (Applied Physics & Engineering) 2025 26(1):1-20
www.jzus.zju.edu.cn; www.springer.com/journal/11582
E-mail: jzus_a@zju.edu.cn

Research Articles

https://doi.org/10.1631/jzus.A2400271

Co-removal potential of heavy metals and dyes from wastewater by simultaneous adsorption with biomass residue formed from microbial treatment of lacquer residue

Xinyue LU[1], Min LIAO[1]✉, Xiaomei XIE[2]✉, Hao QIU[1], Feng YUAN[1], Zhe LUO[1], Chunlin FAN[3]

[1]*Zhejiang Key Laboratory of Agricultural Resources and Environment, College of Environmental and Resource Science, Zhejiang University, Hangzhou 310058, China*
[2]*Experimental Teaching Center, College of Environmental and Resource Science, Zhejiang University, Hangzhou 310058, China*
[3]*Ningbo Ferno Biotechnology Co., Ltd., Ningbo 315502, China*

Abstract: This study aims to optimize the use of lacquer residue biomass (LBM). We investigated the ability of LBM to remove Pb^{2+} heavy metal ions and the typical cationic dye methylene blue (MB) and anionic dye Congo red (CR) by simultaneous adsorption from composite systems, as well as the relevant factors. Scanning electron microscopy (SEM), X-ray diffraction (XRD), and Fourier transform infrared spectroscopy (FTIR) were used to characterize adsorption behavior. The adsorption kinetics of Pb^{2+}-MB/CR composite systems can be effectively characterized by the pseudo-second-order kinetic model (R^2> 0.97). In the Pb^{2+}-MB composite system, adsorption was antagonistic with similar adsorption sites. However, in the Pb^{2+}-CR composite system, we found that adsorption was synergistic with different adsorption sites, which led to a higher simultaneous adsorption capacity for a higher initial Pb^{2+}-CR concentration, unlike the Pb^{2+}-MB system. In both composite systems, an appropriate increase in LBM dosage and system temperature within a certain range was conducive to simultaneous adsorption and removal of Pb^{2+}-MB/CR composite systems. The optimal solid–liquid ratio and temperature were 1∶75 and 30 °C, respectively. The adsorption and removal rates of Pb^{2+} and MB were 99.98% and 90.49%, respectively, and those of Pb^{2+} and CR were 93.99% and 77.39%, respectively, in (50, 50) mg/L of Pb^{2+}-MB/CR composite systems under these conditions. Adsorption removal of Pb^{2+} and MB improved with higher pH levels, and worsened with the increase of ionic strength in the solution, while the removal rate of CR showed an opposite trend. The coexisting anion and cation types had limited influence on the simultaneous adsorption removal of Pb^{2+}, MB, and CR. The results of desorption showed that LBM can be utilized as a disposable material for simultaneously treating Pb^{2+}-MB/CR composite systems. The simultaneous adsorption mechanisms of Pb^{2+}-MB/CR mainly involved hydrogen bonding, π–π bonding interaction, and electrostatic interaction.

Key words: Lacquer residue biomass (LBM); Lead; Methylene blue (MB); Congo red (CR); Simultaneous adsorption removal

1 Introduction

With the ongoing urbanization and industrialization in China, large quantities of wastewater are continuously released into the aquatic ecosystem, including organic and inorganic pollutants, pesticides, heavy metals, and dyes. Because dyeing and printing are major industries in the country, the wastewater from the Chinese textile-dyeing and printing sector constitutes a significant proportion (approximately 40%) of the overall volume of industrial wastewater released. Synthetic dyes are the main pollutants (Cai, 2018; Ye et al., 2020a, 2020b, 2024; Lin et al., 2023). Due to their unique chemical properties, they possess characteristics such as a wide range of pollutants, long duration, and resistance to biodegradation. Cr, Pb, Cu, Ni, Fe, Zn, Hg, Cd, and other heavy metal elements remain in wastewater as well. Catalysts, mordants, and metal antimicrobial additives are all sources of these heavy metals (Li SQ et al., 2019; Cang et al., 2021; Song et al., 2023). Most heavy metals, dyes, and dye metabolites accumulate in large quantities in

✉ Min LIAO, liaomin@zju.edu.cn
Xiaomei XIE, xiexiaomei@zju.edu.cn
Min LIAO, https://orcid.org/0000-0001-9078-204X

Received May 24, 2024; Revision accepted Aug. 4, 2024;
Crosschecked Dec. 16, 2024

animals, humans, and the environment, which can cause extensive damage to humans and ecosystems even at low concentrations. In the past, treatment of such compound-polluted wastewater was often characterized by a combination of several methods, which was cumbersome and costly. Therefore, it is critical to reasonably design and develop a single material for the simultaneous removal of compound pollutants.

Current methods for removing heavy metals and dyes from wastewater include chemical precipitation, ion exchange, photocatalytic degradation, advanced oxidation processes, and adsorption; or combinations of these techniques (Kim et al., 2021; Ma et al., 2021; Li et al., 2022). Adsorption technology is widely used because of its high efficiency, low cost, easy operation, energy savings, and sustainability (Alorabi and Azizi, 2023). At present, biomass materials from various byproducts and wastes left by industrial, agricultural, and forestry production are seen as potential adsorption materials because of their economic accessibility and sustainability. The surface of these byproducts has a porous structure and contains rich active functional groups such as aminos, carboxyls, and hydroxyls, as well as organic matter such as cellulose, amino acids, lipids, and other substances that have strong interactions with anionic and cationic dyes, and heavy metals. This results in excellent adsorption properties with regard to heavy metals and dyes. Many biomass materials have been used in composite pollution systems with heavy metals and dyes, such as cellulose materials, bagasse, fruit peel, humus, and solid–waste ash (Xie et al., 2020; Meneses et al., 2022; An et al., 2023; Chen RP et al., 2024). Cyclic venturi bioreactor technology is the latest microbial treatment process developed by our research group, which has been applied in a series of equipment enterprises, including Yanfeng Automotive Decoration System Wuhan Co., Ltd. of China. The lacquer components are fully degraded in operation, but the lacquer residue biomass (LBM) contains more nascent organic matter and virgin mineral fillers that are also rich in functional groups. If LBM can be used, it would not only avoid the risks caused by improper disposal of waste but also meet the "Carbon Peaking and Carbon Neutrality Goals", which offers economic value. LBM has been reported to be a better adsorbent for anionic and cationic dyes in single systems (Lu et al., 2024), but it remains to be investigated whether LBM could serve as an innovative adsorbent for managing wastewater contaminated with both dyes and heavy metals.

In view of this, we used LBM as our research object and selected the heavy metal Pb^{2+}, the cationic dye methylene blue (MB), and the anionic dye Congo red (CR) as the target pollutants to construct simulated composite wastewater systems. We then explored the simultaneous removal ability for Pb^{2+}-MB/CR composite systems as well as the interactions between Pb^{2+} and MB or CR.

This approach revealed the application potential of LBM, with a view to offering an affordable, readily accessible, and ecological biomass material for concurrent remediation of heavy metals and dyes in wastewater, and also using a "waste resource".

2 Materials and methods

2.1 Reagents and instruments

Chemical reagents: MB, CR, $Pb(NO_3)_2$, H_2SO_4, HNO_3, HCl, and NaCl were analytically pure and purchased from Sinopharm Chemical Reagent Co., Ltd., China. The structural formulas of MB and CR are shown in Fig. S1 of the electronic supplementary materials (ESM).

Instruments: electronic analytical balance (BSA224 S-CW, Sartorius, Germany), ultraviolet spectrophotometer (UV-2450, Shimadzu, Japan), pH meter (PHS-25, Shanghai Yidian Co., Ltd., China), thermostatic oscillator (HZ-9211KB, Jiangsu Taicang Science and Educations Equipment Factory, China), benchtop low-temperature centrifuge (L-550, Hunan Xiang Yi Laboratory Instrument Development Co., Ltd., China), atomic absorptions spectrometer (NOVAA300, Jena Analytical Instruments AG, Germany), scanning electron microscope (SEM) (SU8010, Hitachi Scientific Instruments Ltd., Japan), X-ray diffractometer (XRD) (Bruker D8 Advance, Bruker Ltd., Germany), Fourier transform infrared spectroscopy (FTIR) (NICOLET iS50FT-IR, Thermo Fisher, USA).

2.2 Source and preparation of LBM

The LBM used here was taken from the recirculating venturi bioreactor in the microbial treatment section for residual spray lacquer mist in Yanfeng Automotive Decoration System Wuhan Co., Ltd. The treatment of this bioreactor was carried out by bacterial

strains including the strain group *Beijerinckia sp.* with adhesive and dispersing properties (LM-W, preservation number: CGMCC No. 17168), *Brachymonas sp.* with flocculation and precipitation properties (LM-R, preservation number: CGMCC No. 17167) (Xie et al., 2021), and the residual product obtained after treatment was dried to produce the LBM biomass used in this experiment, which had a moisture content of 1.00%. Additionally, the dried LBM was sifted through a 100-mesh sieve. The obtained LBM consisted mainly of organic matter (56.24% organic matter and 29.75% protein). Of the major constituent elements, C had the highest mass fraction of 36.79%. There were many mineral fillers from the original lacquer in the LBM: the contents of $CaCO_3$, SiO_2, TiO_2, $Fe_2Ti_3O_9$, and $Ca_3(PO_4)_2$ were 34.75%, 0.19%, 5.19%, 1.07%, and 0.78%, respectively. Meanwhile, no content of harmful heavy metals such as Pb, Cd, Zn, Cr, and Cu was detected, and the extractable forms of the above elements in the leachate and dissolved organics were not detected either. Therefore, the LBM could be classified as a material with lower environmental risk. The surface of the LBM was predominantly negatively charged (the pH point of zero charge (pH_{pzc}) was about 4.1) and exhibited relatively moderate pore size, specific surface area, and pore volume. It also had good water permeability, which showed its promise as an adsorbent. Detailed measurements and data sources for the above basic physical and chemical properties of LBM are available in the published literature (Lu et al., 2024).

2.3 Adsorption kinetics of the Pb^{2+}-MB/CR composite systems

LBM was weighed into a series of 50 mL centrifuge tubes (0.20 g per tube), and 15 mL (50, 50) mg/L Pb^{2+}-MB/CR composite system solution (the concentrations of Pb^{2+} and MB or CR were both 50 mg/L) (pH 5.0) was added for adsorption reaction in the thermostatic oscillator at 180 r/min and 30 °C. Samples were taken from the centrifuge tubes at different adsorption-reaction times, and the supernatant was obtained after centrifugation at a speed of 4000 r/min for 10 min. The concentrations of Pb^{2+}, MB, or CR in the supernatant were determined by an atomic absorption spectrometer or ultraviolet spectrophotometer (Azeez et al., 2022; Mu et al., 2022; Wang D et al., 2024). We used the pseudo-first-order kinetic model (Eq. (1)) and pseudo-second-order kinetic model (Eq. (2)) to fit the adsorption data.

$$\ln(q_e - q_t) = \ln q_e - k_1 t, \tag{1}$$

$$\frac{t}{q_t} = \frac{1}{k_2 q_e^2} + \frac{t}{q_e}, \tag{2}$$

where q_e is the adsorption capacity at equilibrium (mg/g); t is the reaction time (min); q_t is the adsorption capacity at time t (mg/g); k_1 and k_2 are the kinetic rate constants (mg/g).

2.4 Isothermal adsorption of the Pb^{2+}-MB/CR composite systems

LBM was weighed into a series of 50 mL centrifuge tubes (0.20 g per tube), and 15 mL Pb^{2+}-MB/CR composite system solution (pH 5.0) with different initial concentrations was added for adsorption reaction in the thermostatic oscillator at 180 r/min and 30 °C. When the adsorption reached equilibrium, the supernatant was obtained after centrifugation at a speed of 4000 r/min for 10 min, and the concentration of Pb^{2+}, MB, or CR in the supernatant was determined. The Langmuir (Eq. (3)) and Freundlich (Eq. (4)) isothermal adsorption models were fitted linearly.

$$\frac{1}{q_e} = \frac{1}{q_{max} K_L} + \frac{C_e}{q_{max}}, \tag{3}$$

$$\ln q_e = \frac{1}{n} \ln C_e + \ln K_F, \tag{4}$$

$$R_L = \frac{1}{1 + K_L C_0}, \tag{5}$$

where C_e is the equilibrium concentration (mg/L); q_{max} is the maximum adsorption capacity of the adsorbent; K_L is the Langmuir constant (L/mg); K_F ((mg/g)·(L/mg)$^{1/n}$) and n are Freundlich constants; C_0 is the highest initial concentration of the adsorbate (mg/L); R_L reflects the affinity of the adsorption process.

2.5 Adsorption thermodynamics of the Pb^{2+}-MB/CR composite systems

To further understand the impact of temperature during adsorption in the Pb^{2+}-MB/CR composite systems, Eqs. (6)–(8) serve to calculate the thermodynamic parameters of the two composite systems, including the Gibbs free energy ($\Delta G°$), enthalpy ($\Delta H°$), and entropy ($\Delta S°$) (Sutar and Jadhav, 2024).

$$K=\frac{C_{\mathrm{ad,e}}}{C_{\mathrm{e}}}, \tag{6}$$

$$\Delta G^{\circ}=\Delta H^{\circ}-T\Delta S^{\circ}, \tag{7}$$

$$\ln K=\frac{\Delta S^{\circ}}{R}-\frac{\Delta H^{\circ}}{RT}. \tag{8}$$

Eq. (6) defines the standard thermodynamic equilibrium constant K (Han et al., 2009). $C_{\mathrm{ad,e}}$ is the concentration of adsorbate on the adsorbent at equilibrium; ΔG° is the Gibbs free energy (kJ/mol); ΔH° is the enthalpy (kJ/mol); ΔS° is the entropy (kJ/(mol·K)); R is the universal gas constant (8.314 J/(mol·K)); T is the reaction temperature (K).

2.6 Influence of system adsorption conditions

We investigated the effect of different adsorption conditions on the adsorption performance of the Pb^{2+}-MB/CR systems ((50, 50) mg/L) with regard to pH (1.0–5.0), background NaCl ionic strength (0.01–0.05 mol/L), LBM dosage (0.05–0.40 g), and adsorption temperature (10–50 °C), based on the monofactor analysis. We then carried out the adsorption reactions in the thermostatic oscillator at 180 r/min. When adsorption reached equilibrium, the supernatant was obtained after centrifugation at a speed of 4000 r/min for 10 min, and the concentration of Pb^{2+}, MB, or CR in the supernatant was determined. The relationship between the solid–liquid ratio and dosage is shown in Table S1 of the ESM.

2.7 Interactions between coexisting pollutants in the composite systems

To explore the interactions between Pb^{2+} and MB or CR in the composite systems, we set the following concentration combinations (Table S2 of the ESM). The composite wastewater of 15 mL described above was added to 50 mL centrifuge tubes containing 0.05 g LBM, and adsorption reaction conditions were the same as described. The supernatant was obtained after centrifugation at a speed of 4000 r/min for 10 min when adsorption reached equilibrium, and the concentrations of Pb^{2+}, MB, or CR in the supernatant were determined. The interaction was evaluated with the ratio of adsorption capacity $R_{\mathrm{q,i}}$ (Eq. (9)) (Du et al., 2022).

$$R_{\mathrm{q,i}}=\frac{q_{\mathrm{m,i}}}{q_{\mathrm{s,i}}}, \tag{9}$$

where $R_{\mathrm{q,i}}$ is the ratio of the adsorption capacity, which is usually categorized into three types: synergistic effect ($R_{\mathrm{q,i}}>1$), indicating a promotional effect within the system; no interaction ($R_{\mathrm{q,i}}=1$), signifying no effect; antagonistic effect ($R_{\mathrm{q,i}}<1$), denoting an inhibitory effect. The adsorption capacities (mg/g) of adsorbate i (Pb^{2+}, MB, or CR) in single and composite systems under the same adsorption conditions are denoted by $q_{\mathrm{s,i}}$ and $q_{\mathrm{m,i}}$, respectively.

2.8 Effect of coexisting anions and cations on adsorption of LBM in the Pb^{2+}-MB/CR composite systems

LBM was weighed into a series of 50 mL centrifuge tubes (0.20 g per tube), and 15 mL (50, 50) mg/L Pb^{2+}-MB/CR composite system solution was added containing Na^{+}, Mg^{2+}, and Ca^{2+} cations (in the form of chloride salt), and CO_3^{2-}, SO_4^{2-}, and PO_4^{3-} anions (in the form of sodium salt) (pH 5.0), with a resulting ionic strength of 0.03 mol/L. The adsorption reactions were carried out in the composite systems in the thermostatic oscillator at 180 r/min and 30 °C. The supernatant was obtained after centrifugation at 4000 r/min for 10 min when adsorption reached equilibrium. Finally, the concentration of Pb^{2+} and MB or CR in the supernatant was determined.

2.9 Calculation of adsorption capacity and adsorption removal rate

The adsorption capacity q (Eq. (10)) and removal rate η (Eq. (11)) can be used to express the effect of adsorption.

$$q=\frac{(C_0-C_{\mathrm{e}})V}{W}, \tag{10}$$

$$\eta=\frac{(C_0-C_{\mathrm{e}})}{C_0}\times 100\%, \tag{11}$$

where V is the volume of the adsorbent solution (L); W is the dosage of LBM (g).

2.10 Desorption of LBM

LBM was weighed into a series of 50 mL centrifuge tubes (0.20 g per tube), and 15 mL (50, 50) mg/L Pb^{2+}-MB/CR composite solution (pH 5.0) was added. The adsorption reactions in the composite systems were carried out in the thermostatic oscillator at 180 r/min and 30 °C. The concentrations of Pb^{2+} and MB or CR

in the supernatant were determined when the adsorption reached equilibrium. We separated the adsorbed-state LBM from the composite systems and obtained the residual liquid volume V_0 by the gravimetric method. Subsequently, 0.1 mol/L H_2SO_4, 0.1 mol/L HNO_3, and 0.1 mol/L HCl of 15 mL were used as desorbents. The desorption reactions were carried out in a thermostatic oscillator at 180 r/min and 30 ℃. After desorption reached equilibrium, the supernatant was obtained after centrifugation at a speed of 4000 r/min for 10 min. The concentration of Pb^{2+}, MB, or CR in the supernatant was determined, and the desorption capacity λ (Eq. (12)) and desorption rate θ (Eq. (13)) were calculated.

$$\lambda = C_t(V_t + V_0) - C_e V_0, \tag{12}$$

$$\theta = \frac{\lambda}{q} \times 100\%, \tag{13}$$

where C_t is the concentration of desorbed adsorbate (mg/L); V_t is the desorbed liquid volume (L); V_0 is the residual liquid volume (L).

2.11 Characterization of adsorption behavior

We observed and analyzed the LBM before and after adsorption with SEM, XRD, and FTIR. The surface morphology characteristics were observed with SEM at an accelerating voltage of 3 kV. The FTIR with the potassium bromide pressurization method was controlled by the frequency range of 4000–400 cm^{-1} with a spectral resolution of 4 cm^{-1} and 32 scans for samples. The XRD measurement conditions were as follows: copper K-alpha, with a tube current and scanning range of 40 mA and 5°–90°, respectively.

3 Results and discussion

3.1 Kinetic characterization of adsorption in Pb^{2+}-MB/CR composite systems

Adsorption is divided into three stages: transportation of the substance from the liquid phase to the boundary layer at the surface of the adsorbent; attachment to the surface of the adsorbent; penetration into pore spaces. Initially, the rate of adsorption is typically rapid, and then it reaches a constant value (Igberase et al., 2018; Khoee et al., 2024).

It can be observed from Fig. 1a that for the Pb^{2+}-MB system, at the onset of the adsorption process, the adsorption of Pb^{2+} from 0–60 min, of MB from 0–30 min, and the adsorption removal rate of Pb^{2+} and MB by LBM increased linearly as the fast adsorption process was extended. The adsorption removal rates of Pb^{2+} and MB reached 88.18% and 73.24% within 60 min and 30 min, respectively. The adsorption rate depends on the availability of adsorption sites (Changalvaei et al., 2021; Nizam et al., 2024). Therefore, the fast adsorption rate and high removal efficiency we observed can be attributed to the large number of surface vacancies on the LBM. Furthermore, the initial concentration during the early phase offered a significant impetus that facilitated the overcoming of mass transfer resistance between the aqueous phase and solid phase for the adsorbate ions (Tattibayeva et al., 2022). With longer times, we observed that the adsorption capacity continued to increase, albeit at a decelerating pace, which indicated a slow reaction process. Adsorption reactions tended to equilibrate after 300 min and finally achieved the maximum adsorption removal. The adsorption removal rates of Pb^{2+}

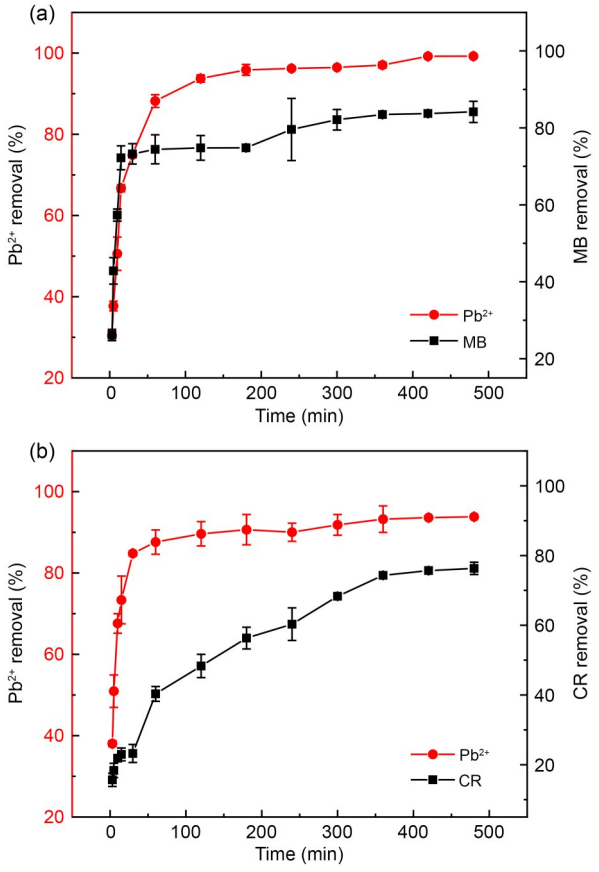

Fig. 1 Effect of adsorption time on LBM adsorption of Pb^{2+}-MB (a) and Pb^{2+}-CR (b) composite systems

and MB by LBM reached 99.23% and 84.16%, respectively. These phenomena can be explained by adsorbate ions gradually occupying the active site of the adsorbent. The enhancement of mass transfer resistance caused by the decrease of adsorbate concentration in the solution might also slow down the adsorption process, causing the adsorption reactions to reach the adsorption equilibrium.

In the Pb^{2+}-CR system (Fig. 1b), when Pb^{2+} and CR were adsorbed for 30 min and 60 min, their adsorption removal rates increased linearly with the prolongation of time, which would also be considered as a fast adsorption process. In comparison to what we saw in the Pb^{2+}-MB system, the adsorption rate of LBM for Pb^{2+} was faster. Therefore, we speculate that coexisting CR has a weaker effect on the adsorption of Pb^{2+}. Compared with MB, the adsorption of CR had a longer adsorption reaction time and relatively lower adsorption removal rate owing to the formation of strong electrostatic attraction between the LBM (negative charge) and the MB (positive charge and cationic type), which promoted faster adsorption of MB. The removal rates of Pb^{2+} and CR increased slowly with longer contact time, indicating a slow reaction process, and the adsorption reactions of both reached equilibrium at 360 min. Finally, the adsorption removal rates of Pb^{2+} and CR reached 93.81% and 76.32%, respectively. It was clear that the adsorption removal rate of Pb^{2+} in the system with a lower initial concentration of Pb^{2+}-MB was slightly higher than in the Pb^{2+}-CR system, but the adsorption removal rates of Pb^{2+} were all higher than 93% in both composite systems. These results might be due to LBM with a negatively charged surface having enough adsorption sites for Pb^{2+} at lower initial concentrations; however, more negatively charged CR was retained in solution by the negative-charge surface repulsion of LBM in the Pb^{2+}-CR system, and sulfonic acid groups on CR in solution could bind to Pb^{2+}, which slightly reduced the adsorption removal rate of Pb^{2+} in the Pb^{2+}-CR system. The structural formula of CR is shown in Fig. S1.

To gain a deeper understanding of the kinetic properties of LBM adsorption in the Pb^{2+}-MB/CR composite systems, we applied both the pseudo-first-order and pseudo-second-order kinetic models to fit the kinetic data (the outcomes are detailed in Table 1). According to the R^2 value of the fitting results, the pseudo-second-order kinetic model provided a more precise representation of the adsorption process for both systems (R^2>0.99). The adsorption capacities predicted by the pseudo-second-order kinetic model for Pb^{2+} and MB were 15.08 mg/g and 3.17 mg/g, respectively, and the predicted data closely aligned with the actual data (14.89 mg/g and 3.16 mg/g). Meanwhile, the adsorption capacities predicted for Pb^{2+} and CR were 14.14 mg/g and 3.04 mg/g, respectively. The predicted data also closely aligned with the actual data (14.07 mg/g and 2.86 mg/g), suggesting that the adsorption reactions in the Pb^{2+}-MB/CR composite systems were controlled by chemical mechanisms (Fan et al., 2018; Lv et al., 2019).

3.2 Isothermal adsorption in Pb^{2+}-MB/CR composite systems

Adsorption isotherms predominantly depict the nature of interactions that occur between the adsorbate and adsorbent, and their relationship. Monolayer molecular adsorption with uniform adsorption capacity on the adsorbent surface is represented well by the Langmuir isotherm model, whereas multilayer molecular adsorption of an adsorbent with an uneven surface-active site suits to the Freundlich isotherm model. Moreover, the energy distribution of the adsorption site decreases exponentially (Kalam et al., 2021; Semwal et al., 2023; Zhang YB et al., 2023). We utilized both isothermal adsorption models to analyze the isothermal adsorption data of Pb^{2+}-MB/CR composite systems, as depicted in Fig. 2 and Table 2.

Table 1 Kinetic parameters of the pseudo-first-order kinetic and pseudo-second-order kinetic

Adsorbate	Concentration (mg/L)	Pseudo-first-order kinetic				Pseudo-second-order kinetic			
		$q_{e,exp}$ (mg/g)	$q_{e,cal}$ (mg/g)	k_1 (min^{-1})	R^2	$q_{e,exp}$ (mg/g)	$q_{e,cal}$ (mg/g)	k_2 (g/(mg·min))	R^2
Pb^{2+}	50	14.89	7.12	0.03	0.88	14.89	15.08	0.01	0.99
MB	50	3.16	1.06	0.02	0.88	3.16	3.17	0.04	0.99
Pb^{2+}	50	14.07	3.40	0.01	0.69	14.07	14.14	0.01	0.99
CR	50	2.86	3.10	0.02	0.87	2.86	3.04	0.01	0.97

$q_{e,exp}$ is the adsorption capacity obtained from the experiment; $q_{e,cal}$ is the theoretical adsorption capacity.

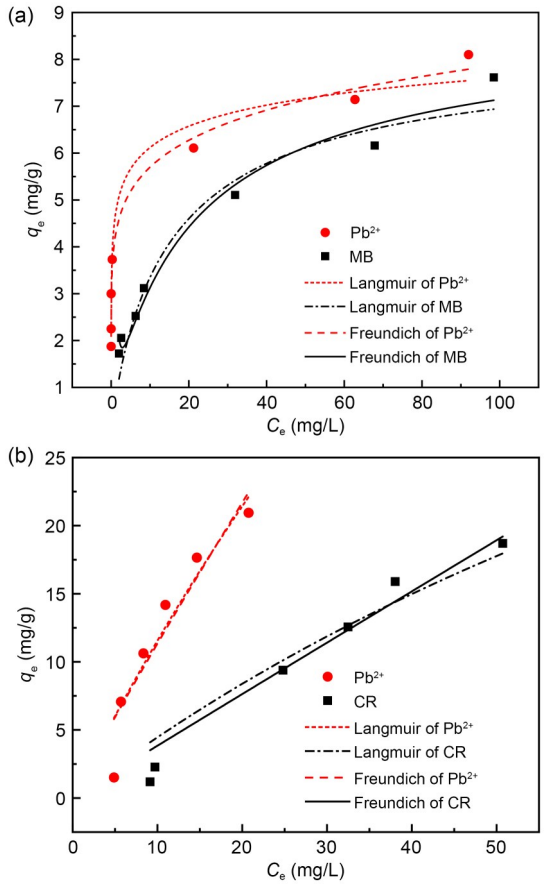

Fig. 2 Langmuir and Freundlich adsorption isotherms of Pb^{2+}-MB (a) and Pb^{2+}-CR (b) composite systems

It can be seen from Fig. 2 and Table 2 that the Langmuir isotherm adsorption model only better characterizes isothermal adsorption of LBM in the Pb^{2+}-MB composite system (R^2>0.97). It exemplifies the intricate nature of adsorption of Pb^{2+}/MB on LBM, arising from diverse chemical interactions such as chemical bonding between adsorbate ions and adsorbent surfaces, and electrostatic forces between adsorbate ions and surface functional groups. The maximum adsorption capacities for Pb^{2+} and MB were 7.63 mg/g and 7.98 mg/g, respectively, at 30 °C. R_L is a non-dimensional equilibrium parameter representing the equilibrium adsorption behavior, which can reflect whether the adsorption process is irreversible (R_L=0), favorable (0<R_L<1), linear (R_L=1), or unfavorable (R_L>1). The results of R_L revealed that the adsorption of Pb^{2+} and MB was a favorable adsorption process on LBM, which meant that Pb^{2+} and MB had a high affinity with the LBM (Table 2). By contrast, the Freundlich isothermal adsorption model had better fitting results for Pb^{2+}-MB (R^2>0.95) or Pb^{2+}-CR (R^2>0.90) composite systems simultaneously adsorbed by LBM. This model accounts for multilayer adsorption, in which the heat of adsorption and affinity are not uniformly distributed on a non-homogeneous surface (Hajiahmadi et al., 2024). The intensity of the interactions between the adsorbate and adsorbent can be inferred from the surface heterogeneity factor 1/n. If 1/n tends towards 0, this indicates that it might be more heterogeneous in nature; if it is 0<1/n<1, this signifies that the level of adsorption is favorable; if 1/n=1, it implies that adsorption is independent of the adsorbent concentration. Conversely, if 1/n>1, adsorption is unfavorable and the affinity is weak (Alorabi and Azizi, 2023; Debnath and Das, 2023; Mondal et al., 2024). We found that the 1/n value was less than 1 for Pb^{2+}-MB/CR composite systems, which suggested that the adsorption processes in Pb^{2+}-MB/CR were effective and the complex multi-layer adsorption processes were dominated by chemisorption (Selim et al., 2018). The above results show that the adsorption performance of LBM for Pb^{2+}-MB/CR composite systems might be controlled by different mechanisms.

3.3 Thermodynamics of the Pb^{2+}-MB/CR composite systems

The adsorption thermodynamic parameters of the Pb^{2+}-MB/CR composite systems at different temperatures are shown in Tables 3 and 4. The $\Delta G°$ of Pb^{2+}, MB, and CR in both systems was negative, which confirmed that the adsorption had good spontaneity (Sangor and Al-Ghouti, 2023). Meanwhile, the $\Delta G°$ increased when the temperature rose, which showed that the spontaneity of the process was enhanced.

Table 2 Parameters of Langmuir and Freundlich isothermal adsorption models

Adsorbate	$q_{e,exp}$ (mg/g)	Langmuir isothermal adsorption model				Freundlich isothermal adsorption model		
		q_{max} (mg/g)	K_L (L/mg)	R_L	R^2	K_F ((mg/g)·(L/mg)$^{1/n}$)	1/n	R^2
Pb^{2+}	8.10	7.63	0.60	0.01	0.98	4.17	0.13	0.95
MB	7.61	7.98	0.08	0.05	0.97	1.37	0.37	0.99
Pb^{2+}	14.18	68.30	0.02	0.21	0.89	1.32	0.94	0.90
CR	12.56	86.66	0.01	0.48	0.88	0.39	0.99	0.96

Table 3 Thermodynamic parameters of the Pb^{2+}-MB composite system

Adsorbate	Temperature (K)	$\Delta G°$ (kJ/mol)	$\Delta H°$ (kJ/mol)	$\Delta S°$ (kJ/(mol·K))
Pb^{2+}	293	−12.37	8.39	0.07
	303	−13.08	8.39	0.07
	313	−13.79	8.39	0.07
MB	293	−0.93	57.94	0.20
	303	−2.94	57.94	0.20
	313	−4.95	57.94	0.20

Table 4 Thermodynamic parameters of the Pb^{2+}-CR composite system

Adsorbate	Temperature (K)	$\Delta G°$ (kJ/mol)	$\Delta H°$ (kJ/mol)	$\Delta S°$ (kJ/(mol·K))
Pb^{2+}	293	−3.02	64.15	0.23
	303	−5.32	64.15	0.23
	313	−7.61	64.15	0.23
CR	293	−1.17	32.89	0.12
	303	−2.33	32.89	0.12
	313	−3.49	32.89	0.12

This means that a higher temperature favors adsorption in both systems. $\Delta H°$ was positive, which further proved that the adsorption of Pb^{2+}, MB, and CR by LBM was endothermic. In addition, the positive $\Delta S°$ denoted an increase in the level of stoichiometry at the solid–liquid interfaces in the systems (Angaru et al., 2021; Gupta et al., 2024).

3.4 Influence of system adsorption conditions

3.4.1 Dosage of LBM

Fig. S2 of the ESM shows the comparison of adsorption in Pb^{2+}-MB and Pb^{2+}-CR composite systems with different LBM dosages. It is clear from the figure that the adsorption and removal of Pb^{2+}, MB, and CR rose as the dosage increased, with the amount of adsorbent exerting a stronger effect on the adsorption of MB and CR.

For the Pb^{2+}-MB system, the adsorption removal rate of Pb^{2+} gradually rose from 96.94% to 99.98% when the dosage went from 0.05 g to 0.40 g. With a dosage change from 0.20 g to 0.40 g, the adsorption removal rate increased slowly, by only 0.52%. For MB, when the dosage was 0.40 g, the adsorption removal rate for the different concentrations reached the maximum, rising from 51.80% to 90.49%. This was a result of the significant increase in surface area in contact with LBM and the usability of LBM adsorption sites (Abbasi et al., 2024). While the adsorption capacity of both decreased, Pb^{2+} decreased from 14.54 mg/g to 1.87 mg/g and MB decreased from 7.77 mg/g to 1.70 mg/g. An explanation for this tendency is that the number of active adsorption sites increased when the dosage of adsorbent increased; however, due to the limited adsorbate concentration, the utilization efficiency of these sites was reduced, leading to a decrease in the mass per unit adsorption capacity of LBM (Yang et al., 2023).

For the Pb^{2+}-CR system, when the dosage changed from 0.05 g to 0.40 g, the adsorption removal rate of Pb^{2+} increased from 90.15% to 93.99%. For CR, when the dosage changed from 0.05 g to 0.40 g, the adsorption removal rate increased from 65.55% to 77.39%. When the dosage changed from 0.20 g to 0.40 g, adsorptive removal of Pb^{2+} and CR tended to flatten out. In addition, the adsorption capacity for both Pb^{2+} and CR decreased, from 13.52 mg/g to 1.76 mg/g and 9.83 mg/g to 1.45 mg/g, respectively. Although a higher dosage achieved a better adsorption removal rate, saturation of the active site and avoidance of excessive waste were the keys to obtaining the best economic benefit. Adsorption removal of both Pb^{2+} and CR in the composite systems had good performance when the dosage was 0.20 g, so for the rest of the study, we determined the solid–liquid ratio of 1∶75 to be the best adsorbent dosage.

3.4.2 System pH

The pH of a solution affects the chemical form of metals and the protonation or deprotonation of adsorbates and adsorbents. Therefore, pH is an important factor during the adsorption process (Wang et al., 2019). Taking into consideration the hydroxide precipitation behavior of Pb^{2+} under alkaline conditions, we carried out the adsorption experiments of the Pb^{2+}-MB/CR composite systems at pH 1.0–5.0.

Fig. S3 of the ESM shows that the adsorption removal rate and adsorption capacity of Pb^{2+} and MB in the Pb^{2+}-MB composite system increased with the increase of pH. After the pH increased from 1.0 to 5.0, the adsorption removal rate and adsorption capacity of Pb^{2+} increased from 35.31% and 1.32 mg/g to 99.46% and 3.73 mg/g, and the removal rate and adsorption capacity of MB increased from 4.22% and 0.16 mg/g to 83.10% and 3.12 mg/g, respectively. This could be related to the adsorbent surface charge. When pH was low, the high concentration of H^+ in the solution

readily protonated the adsorbent surface, causing electrostatic repulsion with Pb^{2+}. Changing simultaneously with higher pH, the positive charge on the surface of LBM gradually decreased (pH_{pzc}=4.1). Consequently, the adsorption of Pb^{2+} and MB was driven by electrostatic attraction. Further, the removal rate and adsorption capacity of Pb^{2+} continued slowly increasing and leveled off at pH 4.0–5.0, which implied that the extent of protonation on the adsorbent's surface, along with the competitive adsorption between H^+ and Pb^{2+}, was diminished (Ghafil et al., 2024).

The difference can be seen in Fig. S3b, in which the adsorptive removal of Pb^{2+} and CR show different trends. As the pH rose from 1.0 to 5.0, the adsorption removal rate and adsorption capacity of Pb^{2+} increased from 45.23% and 1.70 mg/g to 93.15% and 3.49 mg/g, respectively. In contrast, those of CR decreased from 89.16% and 3.34 mg/g to 76.32% and 2.86 mg/g, respectively. This is because MB and CR are different types of ionic dyes, and with the rise in pH, the increase of OH^- resulted in electrostatic repulsion between LBM and anionic CR, which were both negatively charged. In addition, it can be seen by comparing Figs. S3a and S3b that pH had a more obvious influence on Pb^{2+}-MB. These results prove that electrostatic attraction is important during adsorption. In particular, the changing trend of Pb^{2+} in the Pb^{2+}-CR system is not significant, demonstrating that other non-electrostatic interaction factors also contribute to adsorption, for example, π–π packing and hydrogen bonding forces (Li PP et al., 2024). In conclusion, an appropriate increase in pH was favorable for adsorption in the Pb^{2+}-MB composite system, while the best pH was 5 for the Pb^{2+}-CR composite system.

3.4.3 Ionic strength

Ionic strength is another key factor that affects interactions between the adsorbate and the interface of an adsorbent. In general, the effect of ionic strength is mainly manifested as: (1) changes in the structure of the adsorbent bipolar layer; (2) a decrease in the radius of hydrated ions; (3) competition for active sites between coexisting ions (Wang et al., 2013; Chen L et al., 2024).

For the Pb^{2+}-MB system, the adsorption removal and adsorption capacity of Pb^{2+} and MB decreased with the increase of ionic strength (Fig. S4a of the ESM). When NaCl increased from 0.01 mol/L to 0.05 mol/L, the adsorption removal and adsorption capacity of Pb^{2+} and MB decreased by 1.33%, 0.05 mg/g, and 26.78%, 1.00 mg/g, respectively. This further proves that the surface of LBM is mainly characterized by a negative charge. The main reason for these results is that the competition of electrolyte ions caused electrostatic bonding between higher concentrations of Na^+ and LBM (Khodabakhshi et al., 2022; Liu S et al., 2022).

For the Pb^{2+}-CR system (Fig. S4b), the adsorption removal rate and adsorption capacity of Pb^{2+} increased slightly with the ionic strength, from 94.83% and 3.56 mg/g to 97.56% and 3.66 mg/g, respectively, after which there was a decrease of 1.27% and 0.05 mg/g; whereas for CR, the adsorption removal rate and adsorption capacity also increased and then decreased slightly with the increase of ionic strength, from 76.87% and 2.88 mg/g to 78.11% and 2.97 mg/g, respectively, and then decreased by 0.91% and 0.03 mg/g. The removal of Pb^{2+} and CR decreased slightly with the further increase of ionic strength. This might be due to excess ions forming a barrier between LBM and Pb^{2+} and CR (Chanzu et al., 2019; Tang et al., 2020).

Overall, higher ionic strength had less effect on Pb^{2+} and CR. In the case of the anionic dye CR, the presence of Na^+ neutralized the anionic negative charge of CR and weakened the electrostatic repulsion; thus, it facilitated the migration of the anionic dye from the solution to the surface of LBM. In addition, the "salt-out" effect promoted the adsorption of CR (Liu Y et al., 2022). The increase in CR adsorption promoted the adsorption of Pb^{2+} to a certain extent. This is due to the bridge bonding between Pb^{2+} and CR. This synergistic effect was also clarified subsequently. In both composite systems, the adsorption removal of Pb^{2+} exhibited good performance, which also verified the existence of chemisorption between Pb^{2+} and LBM. We speculate that the adsorption force of Pb^{2+} and LBM was too strong to allow desorption. In conclusion, an appropriate reduction of ionic strength for the Pb^{2+}-MB composite system, but an increase of ionic strength for the Pb^{2+}-CR composite system, are conducive to co-adsorption.

3.4.4 System temperature

The effect of temperature can be observed in Fig. S5 of the ESM. In the Pb^{2+}-MB system, LBM had a high adsorption removal rate for Pb^{2+} in 10–50 °C. This implies that LBM has a strong affinity for Pb^{2+}, with a large number of unoccupied adsorption

sites at the beginning which can adsorb rapidly in spite of the lower temperature. As the temperature rose, the adsorption removal rate of Pb^{2+} showed a slightly increasing trend, and the adsorption removal and adsorption capacity increased from 99.11% and 3.72 mg/g to 99.58% and 3.73 mg/g, respectively; for MB, the adsorption efficiency reached the maximum at 40 ℃, with the adsorption removal and adsorption capacity increasing from 49.16% and 1.84 mg/g to 84.336% and 3.16 mg/g, respectively. Then they slightly decreased at 50 ℃ (by 10.87% and 0.41 mg/g). For the Pb^{2+}-CR system, the adsorption removal and adsorption capacity of Pb^{2+} and CR increased with increasing temperature from 70.51% and 2.64 mg/g to 94.96% and 3.56 mg/g, and from 48.50% and 1.87 mg/g to 78.37% and 2.94 mg/g, respectively.

The higher reaction temperature enhanced the thermal movement of molecules and promoted their adsorption capacity. In addition, the increase in temperature led to a decrease in the viscosity of the adsorption solution, thus facilitating the adsorption removal rate. One possible explanation for the slight decrease in adsorption removal and adsorption capacity for MB at 50 ℃ may be the increase in molecular mobility that promoted the desorption of previously adsorbed MB (Abegunde et al., 2024). Alternatively, at higher temperatures, the hydrogen bonds between MB and LBM might be severed, leading to reduced adsorption capacity, as found by Aryee et al. (2022). The increase in the system temperature generally promoted the adsorption capability of LBM, which further highlighted the fact that within a certain temperature range, adsorption of Pb^{2+}, MB, and CR is mainly a heat-absorbing process, in concordance with the laws of adsorption thermodynamics. In brief, an appropriate increase in temperature for Pb^{2+}-MB/CR composite systems is favorable for adsorption.

3.5 Interactions between coexisting pollutants in composite systems

3.5.1 Interaction between Pb^{2+} and MB in a composite system

The results of the interaction between Pb^{2+} and MB in simultaneous adsorption are shown in Fig. S6 of the ESM. Fig. S6a illustrates that with an increase in MB concentration (50 mg/L, 100 mg/L, and 150 mg/L), the adsorption capacity of Pb^{2+} at different concentrations (50 mg/L, 100 mg/L, and 150 mg/L) decreased by 0.93 mg/g, 1.82 mg/g, and 2.04 mg/g, respectively. Meanwhile, with an increase in the concentration of Pb^{2+} (50 mg/L, 100 mg/L, and 150 mg/L), the adsorption capacity of MB at different concentrations (50 mg/L, 100 mg/L, and 150 mg/L) decreased by 2.53 mg/g, 3.70 mg/g, and 6.43 mg/g, respectively (Fig. S6c). We can conclude that in the composite system, Pb^{2+} and MB had the same negatively charged adsorption sites; thus, there were different degrees of antagonism between them. Because some active sites of LBM might be occupied after the adsorption of one component, the spatial site resistance is enhanced, which leads to the adsorption of the other component being further reduced. Certainly, the inhibition of adsorption of another component became more obvious as the concentration of the competing component increased. The reason could be that increasing the concentration of the composite system provided a higher possibility of contact between the active site and the adsorbate. When the adsorption sites on the LBM surface were almost occupied, this caused large numbers of adsorbate ions to compete for the relatively small number of available sites until adsorption saturation was reached.

Cationic dyes and heavy metal ions mainly involve cationic complexation with each other in simultaneous removal, so their diffusion rate to LBM was low and they competed with each other (Visa et al., 2010). Therefore, there was hardly any synergistic or independent adsorption in the composite system of Pb^{2+} and MB. On the one hand, given the electronegativity of LBM, the same positive charge of Pb^{2+} and MB made it possible to have similar adsorption sites. On the other hand, Pb^{2+} would also have electrostatic repulsion with MB. Meanwhile, the inhibitory effect of the two components was different, and the adsorption removal rate of Pb^{2+} was always high, above 96.94%; in other words, the inhibitory effect of MB on the adsorption removal rate of Pb^{2+} was not obvious. This indicates that LBM has enough adsorption sites for Pb^{2+} to adsorb at this concentration. Compared with MB, the adsorption removal rate of Pb^{2+} by LBM was greater. The above implies that the adsorption removal of Pb^{2+} by LBM was in a favorable position in the competitive adsorption. This outcome stems from the variations in the electronic structure and size of Pb^{2+} and MB. Research has indicated that ions with higher charge densities tend to have higher exchange

rates. The positive charge of Pb^{2+} was greater than the number of MB ions, while the spatial structure of Pb^{2+} was smaller than that of MB. These characteristics were more favorable for ion exchange (Wang and Ariyanto, 2007). A comparable observation was made by Liang et al. (2020) regarding the competitive adsorption between MB and Cu^{2+}, which they investigated by utilizing magnetic graphene oxide/alginate microbeads (mGO/CA). They found that since the hydrated ionic radius of Cu^{2+} was smaller than that of MB and the charge density was higher than that of Cu^{2+}, mGO/CA could adsorb much more Cu^{2+} than MB (Liang et al., 2020). Alinezhad et al. (2020) obtained a higher maximum adsorption capacity of Hg^{2+} than MB in binary aqueous solution by using new polymer composites.

At a lower Pb^{2+} concentration (50 mg/L), the $R_{q,Pb}$ was close to 1.0, so the MB had less effect on the adsorption of Pb^{2+} (Fig. S6b). This meant that the adsorption sites of LBM were relatively adequate under these conditions and LBM still removed Pb^{2+}, even in the presence of competing components. However, as the concentration of Pb^{2+} increased, $0.72<R_{q,Pb}<0.97$, which further showed that the inhibitory effect was strengthened when Pb^{2+} concentration was higher. Combined with $0.39<R_{q,MB}<0.64$ (Fig. S6d), the inhibitory effect of MB adsorption by Pb^{2+} was stronger. In a word, LBM had a stronger affinity for Pb^{2+} than MB in the composite system.

3.5.2 Interaction between Pb^{2+} and CR in a composite system

The results of the interaction between Pb^{2+} and CR in simultaneous adsorption are shown in Fig. S7 of the ESM. In Fig. S7a, it can be seen that with the increase of CR concentration (50 mg/L, 100 mg/L, and 150 mg/L), the adsorption capacity of Pb^{2+} at different concentrations (50 mg/L, 100 mg/L, and 150 mg/L) increased by 0.15 mg/g, 0.96 mg/g, and 2.07 mg/g, respectively. With the increase in Pb^{2+} concentration (50 mg/L, 100 mg/L, and 150 mg/L), the adsorption capacity of MB at different concentrations (50 mg/L, 100 mg/L, and 150 mg/L) increased by 1.11 mg/g, 2.38 mg/g, and 5.94 mg/g, respectively (Fig. S7c). Thus, there was a synergistic effect between CR and Pb^{2+}. Clearly, when the concentration of one component increased, it promoted the adsorption process of the other component within a certain concentration range, gradually enhancing the promotion effect. The subsequent process predominantly contributed to the simultaneous adsorption of anionic dyes and heavy metal ions. Initially, the anionic dyes had the potential to engage in complexation with the heavy metal ions and be adsorbed. Then, a certain component preferentially occupied the active site and acted as a bridge to promote the adsorption of other components through coordination, complexation, or electrostatic attraction; for example, the carboxyl, amino, or sulfonic acid groups of the dye molecule could be used as binding sites (Qin et al., 2019). Therefore, in the Pb^{2+}-CR composite system, LBM could still effectively adsorb Pb^{2+} and CR, and the adsorption effect on Pb^{2+} was better. That was because the electrostatic attraction between the negative charge on the LBM surface and Pb^{2+} would lead the migration of Pb^{2+} to the LBM surface, which neutralized the negative charge on the LBM surface. Then, the adsorbed Pb^{2+} could promote the adsorption of negatively charged CR through the bridge bond. Similarly, the adsorbed CR could further adsorb Pb^{2+} through bridge bond. In addition, the hydroxyl, amino, and sulfonic acid groups carried by CR and LBM combined with H^+ in the solution to increase the adsorption of H^+, which in turn reduced H^+ in the solution and enhanced the pH of solution. It resulted in gradual expression of a positively charged state on the surface of LBM, and the adsorption of CR was also promoted by electrostatic attraction. In brief, this synergistic adsorption effect in the form of bridge bond enhanced the adsorption efficiency of Pb^{2+} and CR (Liu et al., 2023). In addition, some of the Pb^{2+} could bind to CR, and LBM with a negatively charged surface had enough adsorption sites for Pb^{2+} at lower initial concentrations. The parts of CR and LBM with negative charge repelled each other and CR was retained in solution, so sulfonic acid groups on CR in solution could interact with Pb^{2+}. At the lower initial concentration of 50 mg/L, $R_{q,Pb}<1.0$, possibly because LBM had an adequate number of adsorption sites for Pb^{2+} and the synergistic effect of the coexisting CR was not significant. With the increase of initial Pb^{2+} concentration, $1.08<R_{q,Pb}<1.38$, and the promotion effect of CR showed an upward trend. This synergistic relationship was also corroborated by the fact that $1.05<R_{q,CR}<1.35$, as shown in Fig. S7d.

3.6 Influence of coexisting cations and anions on adsorption in composite systems

Printing and dyeing wastewater usually contain other complex components that come from various chemical auxiliaries used in dye production and the dyeing process. Therefore, it contains relatively high concentrations of salt substances such as Na^+, Mg^{2+}, K^+, NO_3^-, SO_4^{2-}, and PO_4^{3-}. These cations and anions usually affect adsorption. Therefore, it is of great significance to explore the interference effect of common co-existing ions on adsorption. Figs. S8 and S9 of the ESM show the influence of interfering ions with an ionic strength of 0.03 mol/L in Pb^{2+}-MB/CR composite systems.

In the Pb^{2+}-MB composite system, when cations and anions were added, adsorption and removal of Pb^{2+} were more strongly inhibited by cations than anions; the addition of anions had almost no effect on Pb^{2+}. The coexisting cations had an obvious effect on the adsorption of MB compared to that of Pb^{2+}. For MB, the adsorption removal rate decreased when cations were added. When the ionic strength of Na^+, Mg^{2+}, or K^+ was 0.03 mol/L, the adsorption removal rate of MB decreased by 7.88%, 41.38%, and 48.81%, respectively. However, when anions were added, the adsorption removal rate of MB increased by 0.54%, 1.02%, and 2.81%, respectively. The explanation is that cations and MB have the same positive charge, so they have similar adsorption sites. Cations can occupy the active site of LBM and change its surface electrical properties (Li et al., 2023). However, the addition of anions produced more negative ion sites on the LBM surface, which strengthened the electrostatic attraction with cationic MB. Therefore, the cations inhibited the adsorption removal of MB. At the same time, the impact of interfering cations on MB was in the order of $Na^+<Mg^{2+}<Ca^{2+}$, because the electronegativity as well as the charge of the coexisting ions influenced the adsorption affinity between LBM and MB. Since the charge quantity of Na^+ was less than Ca^{2+} and Mg^{2+}, and the electronegativity of Na^+ (0.93) was less than Ca^{2+} (1.00) and Mg^{2+} (1.31), Ca^{2+} and Mg^{2+} had stronger hydration capacities and electrostatic attraction to easily occupy the active sites (Jiang et al., 2022; Liu et al., 2024). Thus, Ca^{2+} and Mg^{2+} competed more strongly with MB. The influence of interfering anions on MB was in the order of $NO_3^-<SO_4^{2-}<PO_4^{3-}$, indicating that ions with higher valence states had greater potential than univalent ions and carried more negative charge, resulting in a greater influence on MB adsorption (Brahma and Saikia, 2022).

In the Pb^{2+}-CR composite system, the addition of cations and anions promoted the adsorption of Pb^{2+}, with slight increases of 0.78%, 2.77%, 1.92%, 0.68%, 1.17%, and 3.75% after adding 0.03 mol/L of Na^+, Mg^{2+}, Ca^{2+}, NO_3^-, SO_4^{2-}, and PO_4^{3-}, respectively. The addition of cations was beneficial to the adsorption of Pb^{2+}, as the increased adsorption of CR enhanced the negative charge on the surface of LBM, providing additional adsorption sites. The influence of coexisting anions on Pb^{2+} was in the order of $NO_3^-<SO_4^{2-}<PO_4^{3-}$. SO_4^{2-} and PO_4^{3-} easily formed stable precipitation with Pb^{2+}, which reduced the concentration of Pb^{2+} in the form of precipitation; thus, LBM exhibited a higher adsorption removal rate of Pb^{2+}. For CR, when the ionic strength of Na^+, Mg^{2+}, and K^+ was 0.03 mol/L, the adsorption removal rate of CR increased by 7.90%, 12.46%, and 19.78%, respectively. This is due to the fact that the cations in the solution neutralized the repulsive force between the negatively charged LBM and CR. This finding is in alignment with the aforementioned research outcomes regarding the impact of ionic strength. In addition, Mg^{2+} and Ca^{2+} had higher positive charge than Na^+, which explained why Mg^{2+} and Ca^{2+} had a stronger promotion effect, and the "salt-out effect" generated by Mg^{2+} and Ca^{2+} made the precipitated CR more easily adsorbed (Wu ZD et al., 2021). He et al. (2023) also found that Ca^{2+}, Na^+, and K^+ gave activated carbon a positive charge, thus enhancing electrostatic interactions between the adsorbent and CR with high adsorption of CR. In contrast, we found that the anions hindered the adsorption of CR. The influence was in the order of $NO_3^-<SO_4^{2-}<PO_4^{3-}$, and there was a decrease of 15.10%, 19.25%, and 22.91% after adding the 0.03 mol/L NO_3^-, SO_4^{2-}, and PO_4^{3-}, respectively. Because NO_3^-, SO_4^{2-}, PO_4^{3-}, and CR are all anions, they could compete for similar adsorption sites, while NO^{3-}, which had a lower charge density, was less competitive (Sahu et al., 2021). Furthermore, SO_4^{2-} competed with sulfonic acid groups of CR molecules. PO_4^{3-} formed $H_2PO_4^-$, HPO_4^{2-}, and PO_4^{3-} through ionization, which consumed more adsorption sites than other compounds (Brahma and Saikia, 2022; Wu SJ et al., 2022). This resulted in greater inhibition of CR adsorption.

The above results indicate that LBM has the potential to simultaneously adsorb Pb^{2+}, MB, and CR in actual wastewater treatment, especially since it maintains a good adsorption removal rate for Pb^{2+}. They also confirm that electrostatic action plays a crucial role in this adsorption process.

3.7 Desorption characteristics and recycling potential of LBM after adsorption

Optimal recyclability and stability are important features of ideal adsorbent materials (Wang Y et al., 2024b). In order to achieve stability and the potential for LBM regeneration and recycling after adsorption, we tried three different desorbents. The outcome is shown in Fig. S10 of the ESM.

Currently, the usual desorption methods for the regeneration cycle of biomass materials include acid desorption and alkali desorption (Patel, 2021). H^+ displaces large amounts of heavy metal ions and dyes due to competitive adsorption, so regeneration is generally achieved by treating adsorbents in an inorganic acid solution (Lan et al., 2023).

In the Pb^{2+}-MB composite system, the desorption rates of Pb^{2+} were 12.32%, 12.96%, and 9.68%, and the desorption rates of MB were 68.4%, 76.53%, and 83.81% when H_2SO_4, HNO_3, and HCl were respectively used as desorbents. In the Pb^{2+}-CR composite system, the desorption rate of CR was 0%, while the desorption rate of Pb^{2+} was also low. The desorption rates when 0.1 mol/L H_2SO_4, 0.1 mol/L HNO_3, and 0.1 mol/L HCl were used as desorbents were 5.94%, 7.16%, and 5.45%, respectively. The desorption rates of different systems were determined by the structural features of the LBM and the properties of the adsorbate. Biomass with rich functional groups plays a key role in the strong complex adsorption of cationic Pb^{2+} (Li L et al., 2024). Therefore, complexation generated more lead complexes, while the complexation reaction of MB was not evident, resulting in a higher desorption rate for MB than Pb^{2+}. In addition to the possible complexation and chelation between LBM and Pb^{2+}, LBM also contained more minerals such as $Ca_3(PO_4)_2$ and $Fe_2Ti_3O_9$, which formed insoluble precipitates with Pb^{2+} by exchanging ions and removing them as microprecipitation. This led to a portion of the LBM being difficult to desorb, such that the desorption of Pb^{2+} was much less than that of MB. Compared with the Pb^{2+}-MB composite system, desorption of Pb^{2+} in the presence of CR was less, due to the establishment of robust complexes between Pb^{2+} and CR with sulfonic acid groups through electrostatic interaction and coordination (Tran et al., 2022). Meanwhile, the other part of the LBM that adsorbed Pb^{2+} suffered from the promotion of CR, which firmly bonded the Pb^{2+} to the LBM. This explained why Pb^{2+} and CR were more difficult to desorb, and why the LBM that adsorbed Pb^{2+} and CR had better stability. In view of this, LBM could be utilized as a disposable material for simultaneous adsorption removal of Pb^{2+}-CR. Although the Pb^{2+}-MB composite system could be desorbed, the desorption rate was not high and there was a substantial difference between the two systems. The time and cost required for the desorption process lead to the conclusion that LBM as a treatment in the Pb^{2+}-MB composite system is also more suitable as a disposable material. In addition, attention should be paid to avoiding the release of Pb^{2+}, MB, and CR in the treatment of post-adsorption LBM material, because the material had a certain desorption rate, which meant that pollutants might be released from the adsorbent surface into the environment when rainwater leached, leading to secondary pollution.

The mechanism of the adsorption process is also closely related to the desorption process. If an adsorbent can be desorbed with water alone, the adsorption bond is usually weak, whereas desorption with an acid or alkali desorbent is more difficult, showing that stronger chemisorption has occurred. LBM clearly exhibited chemisorption of Pb^{2+}, MB, and CR.

3.8 Characterization of adsorption behavior

3.8.1 Surface characteristics of LBM before and after adsorption in composite systems

SEM was used to scan the surface characteristics as shown in Fig. 3. It is clear that the surface of LBM without adsorption presents an irregular and uneven cluster-like morphology at the microscopic level, rich in crystalline substances. The various particles also have pores of different sizes (Fig. 3a). The uneven folds and porous structure could provide abundant active adsorption sites and promote the efficiency of interactions in pores.

After adsorption in Pb^{2+}-MB/CR composite systems (Fig. 3), LBM has an obvious honeycomb structure and rough cavities, and many sheets and broken structures have formed on the surface because Pb^{2+},

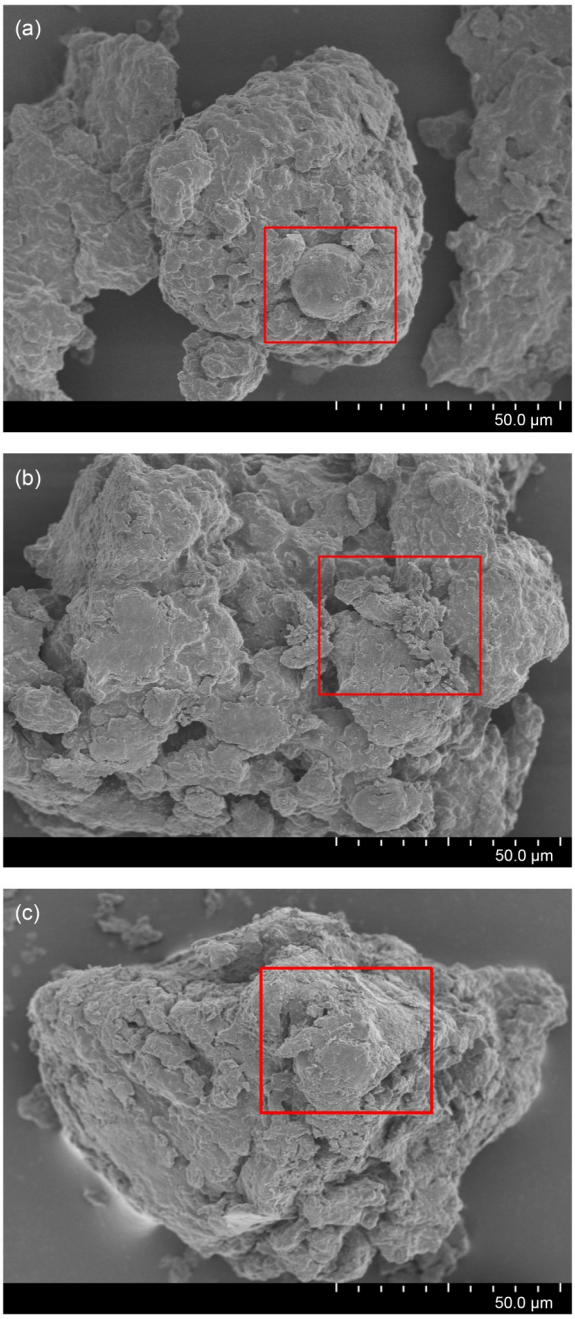

Fig. 3 Surface characteristics of LBM before (a) and after adsorption of Pb^{2+}-MB (b) and Pb^{2+}-CR (c) composite systems

MB, and CR have entered the adsorption sites and destroyed the surface structure. Due to the interaction between the adsorbates and LBM, the adsorbates aggregated on the surface of LBM, which made the surface rougher and looser and formed irregular dispersed shapes. The specific surface area and pore volume of LBM are small, so the pore structure is not the primary controlling factor for adsorption with LBM. The primary factor is surface adsorption, and these results coincide with those obtained via SEM.

3.8.2 XRD characteristics of LBM before and after adsorption in the composite systems

In order to understand the contributions of mineral components in LBM during the adsorption process, we used XRD to analyze LBM before and after adsorption in the composite systems, and the results are shown in Fig. 4. LBM before and after adsorption has obvious characteristic peaks at 27.40°, 28.28°, 36.10°, 41.10°, 43.94°, 54.20°, 56.40°, 62.61°, 63.88°, 68.80°, and 69.61°, which correspond to the characteristic peaks of TiO_2. In addition, 27.40° indicates the characteristic diffraction peak of SiO_2. 36.81°, 39.11°, 41.23°, 54.30°, and 56.61° indicate the characteristic diffraction peaks of $Fe_2Ti_3O_9$. 39.11° is the characteristic diffraction peak of $Ca_3(PO_4)_2$, and 35.96° and 56.61° are the characteristic diffraction peaks of $CaCO_3$.

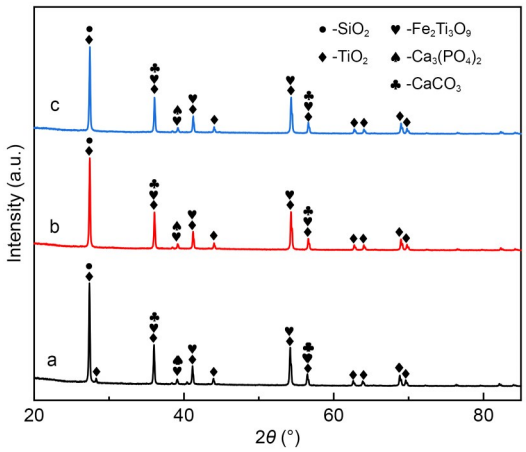

Fig. 4 XRD characteristics of LBM in the Pb^{2+}-MB/CR composite systems before and after adsorption (a: before adsorption; b: after adsorption of Pb^{2+}-MB; c: after adsorption of Pb^{2+}-CR)

Compared with the post-adsorption LBM, the corresponding characteristic peaks shown by LBM before adsorption were sharper and the peak height was higher, meaning that the crystallinity of related minerals was higher. After adsorption, the peak heights of the relative features of LBM decreased, and so did the intensity of the peaks, due to the adsorption reaction between the mineral surfaces in the LBM and the adsorbate molecules during the adsorption process which changed the surface structure of the LBM. This caused

the mineral crystals of the aforementioned minerals to change to an amorphous and loose structure, which resulted in a decrease in the crystallinity of the minerals in the outer layer of the LBM. The small peak at about 28.28° represents TiO_2, which decreased significantly after adsorption, indicating that it played an important role in adsorption. Moreover, SiO_2 and TiO_2 had many surface adsorption sites. Pb^{2+}, MB, and CR were adsorbed in the vacancy through physical adsorption, and hydroxyl produced by hydration acted on Pb^{2+} and both dyes. In addition, SiO_2, $Fe_2Ti_3O_9$, TiO_2, and $Ca_3(PO_4)_2$ facilitated the adsorption of Pb^{2+}, MB, and CR by LBM through bridge bonds. The Ca^{2+} in LBM reacted with the sulfonic acid groups in the anionic dye CR, resulting in precipitation of adsorption. In LBM, the anionic phosphate in $Ca_3(PO_4)_2$ also reacted with MB and Pb^{2+}, forming a stable structure. This also explains the incomplete or very low desorption of MB, CR, and Pb^{2+} after adsorption.

3.8.3 FTIR characteristics of LBM before and after adsorption in the composite systems

LBM contains abundant C, N, O, H, and other elements as well as organic matter, indicating that it contains more organic matter such as microbial residues and microbial metabolites, which would inevitably participate in the adsorption process. In order to understand the adsorption action between the relevant functional groups on LBM and the adsorbent, we used FTIR to analyze the LBM before and after adsorption (Fig. 5).

In the composite systems, due to the interactions between different functional groups and components, the different types of adsorption processes were complicated. It can be seen from Fig. 5 that the infrared absorption peaks of most groups shifted, implying that they reacted with the adsorbate. For the Pb^{2+}-MB composite system, at the peak of 3318 cm^{-1}, the stretching vibration peaks of –OH and N–H shifted to 3394 cm^{-1}. The C=O stretching vibration peak shifted to 1726 cm^{-1}, the –COOH and C=N stretching vibration peaks shifted to 1686 cm^{-1}, and the C=C skeletal vibration peak shifted to 1550 cm^{-1}. Meanwhile, for the Pb^{2+}-CR composite system, the O–H and N–H stretching vibration peaks at 3318 cm^{-1} shifted to 3415 cm^{-1}. The peak at 1685 cm^{-1} can be ascribed to –COOH stretching vibration groups. The C=N stretching vibration groups shifted to 1687 cm^{-1} and the

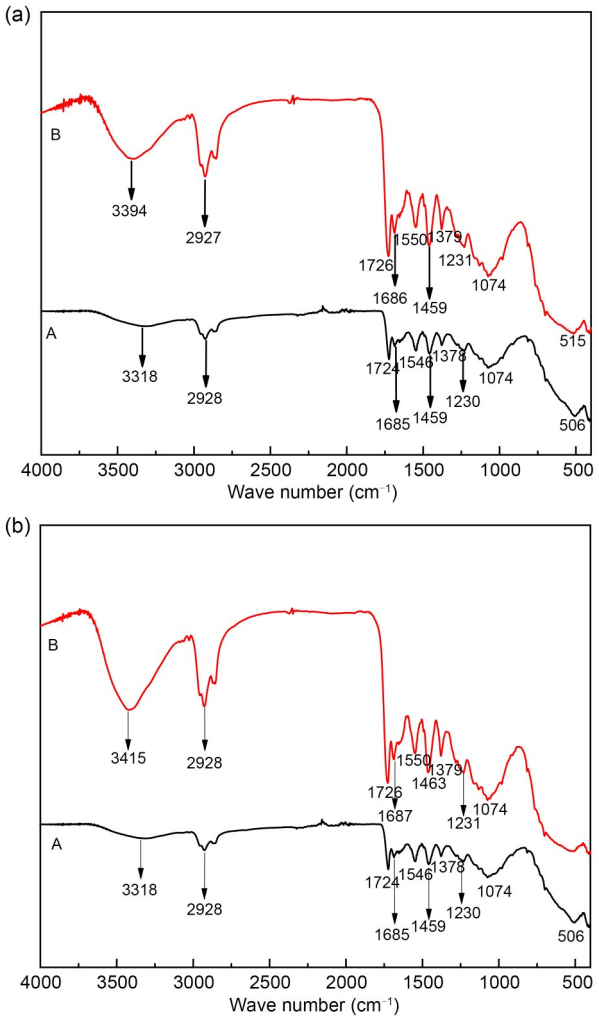

Fig. 5 FTIR characteristics of LBM in Pb^{2+}-MB (a) and Pb^{2+}-CR (b) composite systems (A: before adsorption; B: after adsorption)

C=C skeleton vibration peak of 1546 cm^{-1} shifted to 1550 cm^{-1}. This proves that the abundant amino and carboxyl groups of LBM can form strong complexations with Pb^{2+} and thus have a high adsorption capacity for Pb^{2+}. In addition, O–H (as an electron donor) can form complex with Pb^{2+}, MB, and CR (Kyzas et al., 2015; Li B et al., 2019b). Thus, the hindering effect of complexes was also one of the reasons for the decrease in the adsorption removal rate in the composite system. Combining the molecular structure figures of both dyes (Fig. S1), it can be demonstrated that there are a number of N-containing groups in MB that act as hydrogen bond acceptors. This was linked to the creation of hydrogen bonds with the oxygen-bearing functional groups on LBM, such as hydroxyl, carboxyl, and carbonyl groups. The $–NH_2$, $–SO_3^-$,

and –N=N– groups carried by CR could also form hydrogen bonds with the above-mentioned functional groups on LBM (Li B et al., 2019a; Zhang QY et al., 2023). The bending vibration peaks of $–CONH_2$ at 1378 cm^{-1} and 1230 cm^{-1} after adsorption of the Pb^{2+}-MB composite system shifted to higher wave numbers, and the C–H stretching vibration peak at 506 cm^{-1} weakened significantly and shifted to 515 cm^{-1}. This represented the C–H bending vibration peak at 1459 cm^{-1}, which shifted to 1463 cm^{-1} after adsorption of the Pb^{2+}-CR composite system, and the C–H stretching vibration peak at 506 cm^{-1} disappeared, which can be attributed to complexing reactions during adsorption. Moreover, Pb^{2+}, MB, and CR were adsorbed by hydroxyl groups because of electrostatic interactions, and the aromatic rings on the dye molecule and the C=C double bond carried by CR formed a π–π bonding system with the LBM. Some characteristic peaks such as $–CH_2$ stretching vibration and C=C skeleton vibration peaks were not significantly shifted. However, it is clear that the strength of infrared characteristic peaks was enhanced after adsorption in the two composite systems. Meanwhile, the strength of infrared characteristic peaks of –OH and N–H groups, which were significantly shifted, was also enhanced. These results indicate that some organic substances, i.e., MB and CR, were adsorbed on the LBM surface. This is because in the composite system, the possible interactions between adsorbates and LBM resulted in an increase in the above-mentioned groups due to the adsorbed MB or CR on the LBM surface.

In summary, the positively charged groups (e.g., –OH) and negatively charged groups (e.g., –COOH) carried by LBM achieved synergistic removal of Pb^{2+} and anionic dyes in water by electrostatic attraction. Vibrational changes in the O–H, N–H, and –COOH stretching vibration peaks indicate complexation with Pb^{2+}, MB, and CR; N groups also played an important role as hydrogen receptors and hydrogen bonds with oxygen-containing functional groups such as O–H, –COOH, and C=O carried by LBM. In addition, O–H and C–H stretching vibration peaks, the C=N stretching vibration peak, and the C=C skeleton vibration peak could combine with the MB and CR through non-covalent interactions such as CH–π or π–π conjugated effects. This proves that functional groups such as hydroxyls, aminos, carbonyls, alkyls, and carboxyls, interact with an adsorbent and make important contributions to competitive adsorption.

4 Conclusions

LBM is a suitable, novel material for simultaneous adsorption removal of heavy metals and dyes in the composite system of printing and dyeing wastewater. The adsorption kinetics of Pb^{2+}-MB/CR composite systems can be effectively characterized by the pseudo-second-order kinetic model (R^2>0.97), which is dominated by the chemisorption process. In the Pb^{2+}-MB composite system, both the Langmuir isothermal adsorption model (R^2>0.97) and Freundlich isothermal adsorption model (R^2>0.95) better describe the isothermal adsorption characteristics of Pb^{2+} and MB, while only the Freundlich isothermal adsorption model accurately describes the isothermal adsorption characteristics of Pb^{2+} and CR in the Pb^{2+}-CR composite system (R^2>0.90). In the Pb^{2+}-MB composite system, the adsorption is antagonistic with similar adsorption sites. However, the adsorption is synergistic with different adsorption sites in the Pb^{2+}-CR composite system, which leads to a higher simultaneous adsorption capacity with a higher initial Pb^{2+}-CR concentration than that of Pb^{2+}-MB. In the Pb^{2+}-MB/CR composite systems, an appropriate increase of the LBM dosage and system temperature within a certain range contributes to the simultaneous adsorption removal of Pb^{2+} and MB or CR. The optimal solid–liquid ratio and temperature are 1∶75 and 30 ℃, respectively. The adsorption and removal rates of Pb^{2+} and MB were 99.98% and 90.49%, respectively, and those of Pb^{2+} and CR were 93.99% and 77.39%, respectively, in (50, 50) mg/L of Pb^{2+}-MB/CR composite systems under these conditions. The adsorption removal of Pb^{2+} and MB increases with the pH level and decreases as the ionic strength increases, while the removal rate of CR shows an opposite trend, slowly decreasing with the increase of pH and increasing with the increase of ionic strength.

The coexisting cation and anion types have a limited effect on the simultaneous adsorption removal of Pb^{2+}, MB, and CR. In the Pb^{2+}-MB composite system, the desorption rates of LBM-adsorbed Pb^{2+} and MB were lower than 12.96% and higher than 68.40%, respectively, with a large difference in the desorption

rate; whereas in the Pb^{2+}-CR composite system, the desorption rates of LBM-adsorbed Pb^{2+} and CR were lower than 7.16%, indicating that LBM-adsorbed Pb^{2+} and CR had good stability. Therefore, based on the different adsorption characteristics of LBM in the two systems, we suggest that it could be utilized as a disposable material for simultaneous adsorption and removal of Pb^{2+}-MB/CR composite systems. In addition, the structure and various inorganic and organic components of LBM contribute to simultaneous adsorption and removal. The characterization results reveal that the adsorption of the two composite systems is controlled by complex interactions involving hydrogen bonding, complexations, π–π bonding interactions, and electrostatic interactions.

Acknowledgments

This work is supported by the National Key Research and Development Program of China (Nos. 2023YFD1702003 and 2023YFC3709001).

Author contributions

Xiaomei XIE and Min LIAO conceived the idea and designed the research. Xinyue LU, Hao QIU, Feng YUAN, Zhe LUO, and Chunlin FAN performed the experiment. Xiaomei XIE, Xinyue LU, and Min LIAO analyzed the data and wrote the manuscript. All authors contributed to the discussion of the manuscript.

Conflict of interest

Xinyue LU, Min LIAO, Xiaomei XIE, Hao QIU, Feng YUAN, Zhe LUO, and Chunlin FAN declare that they have no conflict of interest.

Data availability

Data will be made available on request.

References

Abbasi A, Ahmad I, Abd El-Gawad HH, et al., 2024. Appraisal of the adsorption potential of novel modified gellan gum nanocomposite for the confiscation of methylene blue and malachite green. *International Journal of Biological Macromolecules*, 259:129221. https://doi.org/10.1016/j.ijbiomac.2024.129221

Abegunde SM, Olasehinde EF, Adebayo MA, 2024. Green synthesis of ZnO nanoparticles using *Nauclea latifolia* fruit extract for adsorption of Congo red. *Hybrid Advances*, 5: 100164. https://doi.org/10.1016/j.hybadv.2024.100164

Alinezhad H, Zabihi M, Kahfroushan D, 2020. Design and fabrication the novel polymeric magnetic boehmite nanocomposite (boehmite@Fe_3O_4@PLA@SiO_2) for the remarkable competitive adsorption of methylene blue and mercury ions. *Journal of Physics and Chemistry of Solids*, 144: 109515. https://doi.org/10.1016/j.jpcs.2020.109515

Alorabi AQ, Azizi M, 2023. Effective removal of methyl green from aqueous environment using activated residual *Dodonaea Viscosa* : equilibrium, isotherm, and mechanism studies. *Environmental Pollutants and Bioavailability*, 35(1):2168761. https://doi.org/10.1080/26395940.2023.2168761

An CC, Zhang M, Xiao ZH, et al., 2023. Lignocellulose/chitosan hybrid aerogel composited with fluorescence molecular probe for simultaneous adsorption and detection of heavy metal pollutants. *Journal of Environmental Chemical Engineering*, 11(6):111205. https://doi.org/10.1016/j.jece.2023.111205

Angaru GKR, Lingamdinne LP, Choi YL, et al., 2021. Encapsulated zerovalent iron/nickel-fly ash zeolite foam for treating industrial wastewater contaminated by heavy metals. *Materials Today Chemistry*, 22:100577. https://doi.org/10.1016/j.mtchem.2021.100577

Aryee AA, Gao CP, Han RP, et al., 2022. Functionalized magnetic biocomposite based on peanut husk for the efficient sequestration of basic dyes in single and binary systems: adsorption mechanism and antibacterial study. *Journal of Environmental Chemical Engineering*, 10(4):108205. https://doi.org/10.1016/j.jece.2022.108205

Azeez L, Adebisi SA, Adejumo AL, et al., 2022. Adsorptive properties of rod-shaped silver nanoparticles-functionalized biogenic hydroxyapatite for remediating methylene blue and Congo red. *Inorganic Chemistry Communications*, 142:109655. https://doi.org/10.1016/j.inoche.2022.109655

Brahma D, Saikia H, 2022. Synthesis of ZrO_2/MgAl-LDH composites and evaluation of its isotherm, kinetics and thermodynamic properties in the adsorption of Congo red dye. *Chemical Thermodynamics and Thermal Analysis*, 7:100067. https://doi.org/10.1016/j.ctta.2022.100067

Cai L, 2018. Aniline degradation and dye decolorization with mixed bacteria in printing and dyeing wastewater. *China Dyeing and Finishing*, 44(17):39-43 (in Chinese).

Cang JS, Li YJ, Liu DJ, et al., 2021. Separation of trace Pb(II) and Cd(II) in dyeing wastewater by carbon dioxide driven ionic liquid two-phase extraction. *China Dyeing and Finishing*, 47(11):67-70 (in Chinese).

Changalvaei M, Nilforoushan MR, Arabmarkadeh A, et al., 2021. Removal of Ni and Zn heavy metal ions from industrial waste waters using modified slag of electric arc furnace. *Materials Research Express*, 8(5):055506. https://doi.org/10.1088/2053-1591/abf520

Chanzu HA, Onyari JM, Shiundu PM, 2019. Brewers' spent grain in adsorption of aqueous Congo red and malachite green dyes: batch and continuous flow systems. *Journal of Hazardous Materials*, 380:120897. https://doi.org/10.1016/j.jhazmat.2019.120897

Chen L, Hu J, He YY, et al., 2024. Microwave-assisted pyrolysis of waste lignin to prepare biochar for Cu^{2+} highly-efficient adsorption: performance, kinetics and mechanism resolution. *Separation and Purification Technology*, 342:127070.

https://doi.org/10.1016/j.seppur.2024.127070

Chen RP, Gan CH, Cai BC, et al., 2024. Co-adsorption and selective-adsorption of heavy metals and dyes from aqueous solution by bio-based humus/chitosan hydrogels. *Journal of Environmental Sciences*, 145:193-204. https://doi.org/10.1016/j.jes.2023.09.004

Debnath S, Das R, 2023. Strong adsorption of CV dye by Ni ferrite nanoparticles for waste water purification: fits well the pseudo second order kinetic and Freundlich isotherm model. *Ceramics International*, 49(10):16199-16215. https://doi.org/10.1016/j.ceramint.2023.01.218

Du PY, Xu L, Ke ZJ, et al., 2022. A highly efficient biomass-based adsorbent fabricated by graft copolymerization: kinetics, isotherms, mechanism and coadsorption investigations for cationic dye and heavy metal. *Journal of Colloid and Interface Science*, 616:12-22. https://doi.org/10.1016/j.jcis.2022.02.048

Fan C, Liang Y, Dong HQ, et al., 2018. Guanidinium ionic liquid-controlled synthesis of zeolitic imidazolate framework for improving its adsorption property. *Science of the Total Environment*, 640-641:163-173. https://doi.org/10.1016/j.scitotenv.2018.05.282

Ghafil AJ, Mazloom G, Abdi J, et al., 2024. $Ti_3C_2T_x$/ZIF-67 hybrid nanocomposite as a highly effective adsorbent for Pb(II) removal from water: synthesis and DFT calculations. *Applied Surface Science*, 643:158642. https://doi.org/10.1016/j.apsusc.2023.158642

Gupta SV, Kulkarni VV, Ahmaruzzaman M, 2024. Fabrication of a bio-adsorbent material by grafting CeO_2 quantum dots (QDts) over Areca nut shell biochar using Saccharum officinarum extract as a solvent/capping agent for adsorption of methylene blue dye: synthesis, material analyses, adsorption kinetics and isotherms studies. *Colloids and Surfaces A: Physicochemical and Engineering Aspects*, 680:132611. https://doi.org/10.1016/j.colsurfa.2023.132611

Hajiahmadi Z, Moheb A, Mohammadi M, et al., 2024. Surface and mass transfer kinetic and equilibrium modeling of Pb(II) ions adsorption on hydroxyapatite scaffold: batch and fixed-bed column studies. *Separation and Purification Technology*, 343:127141. https://doi.org/10.1016/j.seppur.2024.127141

Han RP, Zhang JJ, Han P, et al., 2009. Study of equilibrium, kinetic and thermodynamic parameters about methylene blue adsorption onto natural zeolite. *Chemical Engineering Journal*, 145(3):496-504. https://doi.org/10.1016/j.cej.2008.05.003

He S, Sun JW, Jin X, et al., 2023. Adsorption enhancement of Congo red dye from wastewater based on edamame shell originated activated carbon by the cations: experimental and theoretical studies. *Diamond and Related Materials*, 136:109930. https://doi.org/10.1016/j.diamond.2023.109930

Igberase E, Osifo P, Ofomaja A, 2018. Adsorption of metal ions by microwave assisted grafting of cross-linked chitosan beads. Equilibrium, isotherm, thermodynamic and desorption studies. *Applied Organometallic Chemistry*, 32(3):e4131. https://doi.org/10.1002/aoc.4131

Jiang J, Huang XY, Bai JL, et al., 2022. Adsorption of clothianidin by potassium permanganate modified biochar in aqueous solution. *Chinese Journal of Environmental Engineering*, 16(4):1175-1185 (in Chinese). https://doi.org/10.12030/j.cjee.202201055

Kalam S, Abu-Khamsin SA, Kamal MS, et al., 2021. Surfactant adsorption isotherms: a review. *ACS Omega*, 6(48): 32342-32348. https://doi.org/10.1021/acsomega.1c04661

Khodabakhshi A, Mohammadi-Moghadam F, Shakeri K, et al., 2022. Equilibrium and thermodynamic studies on the biosorption of lead (II) by living and nonliving biomass of *Penicillium notatum*. *Journal of Chemistry*, 2022: 3109212. https://doi.org/10.1155/2022/3109212

Khoee S, Koohrou SA, Moayeri S, 2024. Use of NIR/$NaBH_4$ combinatorial techniques for simultaneous and high-efficient adsorption of heavy metal ions from contaminated water by Chitosan/Au Janus microdisks. *Surfaces and Interfaces*, 44:103801. https://doi.org/10.1016/j.surfin.2023.103801

Kim SH, Chung H, Jeong S, et al., 2021. Identification of pH-dependent removal mechanisms of lead and arsenic by basic oxygen furnace slag: relative contribution of precipitation and adsorption. *Journal of Cleaner Production*, 279:123451. https://doi.org/10.1016/j.jclepro.2020.123451

Kyzas GZ, Siafaka PI, Pavlidou EG, et al., 2015. Synthesis and adsorption application of succinyl-grafted chitosan for the simultaneous removal of zinc and cationic dye from binary hazardous mixtures. *Chemical Engineering Journal*, 259:438-448. https://doi.org/10.1016/j.cej.2014.08.019

Lan HC, Zhang S, Zhang JY, et al., 2023. Water-soluble carbon nitride as phase-convertible adsorbents for removing heavy metals from water. *Applied Surface Science*, 614: 156172. https://doi.org/10.1016/j.apsusc.2022.156172

Li B, Guo JZ, Lv KL, et al., 2019a. Adsorption of methylene blue and Cd(II) onto maleylated modified hydrochar from water. *Environmental Pollution*, 254:113014. https://doi.org/10.1016/j.envpol.2019.113014

Li B, Lv JQ, Guo JZ, et al., 2019b. The polyaminocarboxylated modified hydrochar for efficient capturing methylene blue and Cu(II) from water. *Bioresource Technology*, 275: 360-367. https://doi.org/10.1016/j.biortech.2018.12.083

Li B, Liu JL, Xu H, 2022. Synthesis of polyaminophosphonated-functionalized hydrochar for efficient sorption of Pb(II). *Environmental Science and Pollution Research*, 29(33): 49808-49815. https://doi.org/10.1007/s11356-022-19350-4

Li L, Bai YF, Qi CH, et al., 2024. Adsorption of Pb(II) and Cu(II) by succinic anhydride-modified apple pomace. *Biochemical Engineering Journal*, 201:109136. https://doi.org/10.1016/j.bej.2023.109136

Li PP, Li Z, Liu SY, et al., 2024. Imidazole/pyridine-based ionic liquids modified metal-organic frameworks for efficient adsorption of Congo red in water. *Journal of Molecular Structure*, 1303:137599.

https://doi.org/10.1016/j.molstruc.2024.137599

Li SH, Luo C, Yan F, et al., 2023. Remediation of Pb(II) and Cd(II) in polluted waters with calcium thioglycolate-modified straw biochar. *Environmental Pollution*, 338: 122638. https://doi.org/10.1016/j.envpol.2023.122638

Li SQ, Fan ZL, Li Q, et al., 2019. Magnetic metal-organic framework material and its application in printing and dyeing wastewater treatment (I). *China Dyeing and Finishing*, 45(22):53-56 (in Chinese).

Liang YQ, Li H, Mao XM, et al., 2020. Competitive adsorption of methylene blue and Cu(II) onto magnetic graphene oxide/alginate beads. *Russian Journal of Physical Chemistry A*, 94(12):2605-2613. https://doi.org/10.1134/S0036024420120158

Lin JY, Ye WY, Xie M, et al., 2023. Environmental impacts and remediation of dye-containing wastewater. *Nature Reviews Earth & Environment*, 4(11):785-803. https://doi.org/10.1038/s43017-023-00489-8

Liu B, Lv P, Wu RF, et al., 2023. Coal gasification fine slag based multifunctional nanoporous silica microspheres for synergistic adsorption of Pb(II) and Congo red. *Separation and Purification Technology*, 323:124478. https://doi.org/10.1016/j.seppur.2023.124478

Liu FJ, He Q, Su L, et al., 2024. Adsorption properties of methylene blue by surface functionalized magnetic biochar with sodium alginate. *Inorganic Chemicals Industry*, 56(2):65-73 (in Chinese). https://doi.org/10.19964/j.issn.1006-4990.2023-0180

Liu S, Huang JH, Zhang W, et al., 2022. Investigation of the adsorption behavior of Pb(II) onto natural-aged microplastics as affected by salt ions. *Journal of Hazardous Materials*, 431:128643. https://doi.org/10.1016/j.jhazmat.2022.128643

Liu Y, Qiu GY, Liu YF, et al., 2022. Fabrication of CoFe-MOF materials by different methods and adsorption properties for Congo red. *Journal of Molecular Liquids*, 360: 119405. https://doi.org/10.1016/j.molliq.2022.119405

Lu XY, Liao M, Xie XM, et al., 2024. The potential of biomass residue formed from microbial treatment of lacquer residue for adsorption and removal of dye from wastewater. *Acta Scientiae Circumstantiae*, 44(4):82-94 (in Chinese). https://doi.org/10.13671/j.hjkxxb.2023.0373

Lv SW, Liu JM, Ma H, et al., 2019. Simultaneous adsorption of methyl orange and methylene blue from aqueous solution using amino functionalized Zr-based MOFs. *Microporous and Mesoporous Materials*, 282:179-187. https://doi.org/10.1016/j.micromeso.2019.03.017

Ma DS, Yi H, Lai C, et al., 2021. Critical review of advanced oxidation processes in organic wastewater treatment. *Chemosphere*, 275:130104. https://doi.org/10.1016/j.chemosphere.2021.130104

Meneses IP, Novaes SD, Dezotti RS, et al., 2022. CTAB-modified carboxymethyl cellulose/bagasse cryogels for the efficient removal of bisphenol A, methylene blue and Cr(VI) ions: batch and column adsorption studies. *Journal of Hazardous Materials*, 421:126804. https://doi.org/10.1016/j.jhazmat.2021.126804

Mondal MIH, Chakraborty SC, Rahman MS, et al., 2024. Adsorbents from rice husk and shrimp shell for effective removal of heavy metals and reactive dyes in water. *Environmental Pollution*, 346:123637. https://doi.org/10.1016/j.envpol.2024.123637

Mu ZH, Liu DN, Lv J, et al., 2022. Insight into the highly efficient adsorption towards cationic methylene blue dye with a superabsorbent polymer modified by esterified starch. *Journal of Environmental Chemical Engineering*, 10(5):108425. https://doi.org/10.1016/j.jece.2022.108425

Nizam T, Krishnan KA, Joseph A, et al., 2024. Isotherm, kinetic and thermodynamic modelling of liquid phase adsorption of the heavy metal ions Zn(II), Pb(II) and Cr(VI) onto $MgFe_2O_4$ nanoparticles. *Groundwater for Sustainable Development*, 25:101120. https://doi.org/10.1016/j.gsd.2024.101120

Patel H, 2021. Review on solvent desorption study from exhausted adsorbent. *Journal of Saudi Chemical Society*, 25(8):101302. https://doi.org/10.1016/j.jscs.2021.101302

Qin XM, Bai L, Tan YZ, et al., 2019. β-cyclodextrin-crosslinked polymeric adsorbent for simultaneous removal and stepwise recovery of organic dyes and heavy metal ions: fabrication, performance and mechanisms. *Chemical Engineering Journal*, 372:1007-1018. https://doi.org/10.1016/j.cej.2019.05.006

Sahu S, Bishoyi N, Sahu MK, et al., 2021. Investigating the selectivity and interference behavior for detoxification of Cr(VI) using lanthanum phosphate polyaniline nanocomposite via adsorption-reduction mechanism. *Chemosphere*, 278:130507. https://doi.org/10.1016/j.chemosphere.2021.130507

Sangor FIMS, Al-Ghouti MA, 2023. Waste-to-value: synthesis of nano-aluminum oxide (nano-γ-Al_2O_3) from waste aluminum foils for efficient adsorption of methylene blue dye. *Case Studies in Chemical and Environmental Engineering*, 8:100394. https://doi.org/10.1016/j.cscee.2023.100394

Selim AQ, Mohamed EA, Mobarak M, et al., 2018. Cr(VI) uptake by a composite of processed diatomite with MCM-41: isotherm, kinetic and thermodynamic studies. *Microporous and Mesoporous Materials*, 260:84-92. https://doi.org/10.1016/j.micromeso.2017.10.041

Semwal N, Mahar D, Chatti M, et al., 2023. Adsorptive removal of Congo red dye from its aqueous solution by Ag-Cu-CeO_2 nanocomposites: adsorption kinetics, isotherms, and thermodynamics. *Heliyon*, 9(11):e22027. https://doi.org/10.1016/j.heliyon.2023.e22027

Song YL, Wang LJ, Qiang X, et al., 2023. An overview of biological mechanisms and strategies for treating wastewater from printing and dyeing processes. *Journal of Water Process Engineering*, 55:104242. https://doi.org/10.1016/j.jwpe.2023.104242

Sutar S, Jadhav J, 2024. A comparative assessment of the methylene blue dye adsorption capacity of natural biochar versus chemically altered activated carbons. *Bioresource Technology Reports*, 25:101726. https://doi.org/10.1016/j.biteb.2023.101726

Tang J, Zhang YF, Liu Y, et al., 2020. Efficient ion-enhanced

adsorption of Congo red on polyacrolein from aqueous solution: experiments, characterization and mechanism studies. *Separation and Purification Technology*, 252: 117445.
https://doi.org/10.1016/j.seppur.2020.117445

Tattibayeva Z, Tazhibayeva S, Kujawski W, et al., 2022. Peculiarities of adsorption of Cr (VI) ions on the surface of *Chlorella vulgaris ZBS1* algae cells. *Heliyon*, 8(9):e10468.
https://doi.org/10.1016/j.heliyon.2022.e10468

Tran CC, Dong HC, Truong VTN, et al., 2022. Enhancing the remarkable adsorption of Pb^{2+} in a series of sulfonic-functionalized Zr-based MOFs: a combined theoretical and experimental study for elucidating the adsorption mechanism. *Dalton Transactions*, 51(19):7503-7516.
https://doi.org/10.1039/d2dt01009g

Visa M, Bogatu C, Duta A, 2010. Simultaneous adsorption of dyes and heavy metals from multicomponent solutions using fly ash. *Applied Surface Science*, 256(17):5486-5491.
https://doi.org/10.1016/j.apsusc.2009.12.145

Wang D, Chen HS, Xin CY, et al., 2024. Insight into adsorption of Pb(II) with wild resistant bacteria TJ6 immobilized on biochar composite: roles of bacterial cell and biochar. *Separation and Purification Technology*, 331: 125660.
https://doi.org/10.1016/j.seppur.2023.125660

Wang J, Gao ML, Shen T, et al., 2019. Insights into the efficient adsorption of rhodamine B on tunable organo-vermiculites. *Journal of Hazardous Materials*, 366:501-511.
https://doi.org/10.1016/j.jhazmat.2018.12.031

Wang SB, Ariyanto E, 2007. Competitive adsorption of malachite green and Pb ions on natural zeolite. *Journal of Colloid and Interface Science*, 314(1):25-31.
https://doi.org/10.1016/j.jcis.2007.05.032

Wang T, Liu W, Xiong L, et al., 2013. Influence of pH, ionic strength and humic acid on competitive adsorption of Pb(II), Cd(II) and Cr(III) onto titanate nanotubes. *Chemical Engineering Journal*, 215-216:366-374.
https://doi.org/10.1016/j.cej.2012.11.029

Wang Y, Yu S, Yuan HW, et al., 2024. Constructing N, S co-doped network biochar confined $CoFe_2O_4$ magnetic nanoparticles adsorbent: insights into the synergistic and competitive adsorption of Pb^{2+} and ciprofloxacin. *Environmental Pollution*, 343:123178.
https://doi.org/10.1016/j.envpol.2023.123178

Wu SJ, Li MY, Xin LL, et al., 2022. Efficient removal of Cr(VI) by triethylenetetramine modified sodium alginate/carbonized chitosan composite via adsorption and photocatalytic reduction. *Journal of Molecular Liquids*, 366: 120160.
https://doi.org/10.1016/j.molliq.2022.120160

Wu ZD, Wang XM, Yao J, et al., 2021. Synthesis of polyethyleneimine modified $CoFe_2O_4$-loaded porous biochar for selective adsorption properties towards dyes and exploration of interaction mechanisms. *Separation and Purification Technology*, 277:119474.
https://doi.org/10.1016/j.seppur.2021.119474

Xie WJ, Pakdel E, Liang YJ, et al., 2020. Natural melanin/TiO_2 hybrids for simultaneous removal of dyes and heavy metal ions under visible light. *Journal of Photochemistry and Photobiology A: Chemistry*, 389:112292.
https://doi.org/10.1016/j.jphotochem.2019.112292

Xie XM, Liao M, Xu N, et al., 2021. A Mixed Bacterial Agent for Degrading Mixed Wastewater of Toluene, Xylene, and Acrylic Acid Water and Its Applications. CN Patent 110591984 B (in Chinese).

Yang W, Kong YD, Yin H, et al., 2023. Study on the adsorption performance of ZIF-8 on heavy metal ions in water and the recycling of waste ZIF-8 in cement. *Journal of Solid State Chemistry*, 326:124217.
https://doi.org/10.1016/j.jssc.2023.124217

Ye WY, Ye KF, Lin F, et al., 2020a. Enhanced fractionation of dye/salt mixtures by tight ultrafiltration membranes via fast bio-inspired co-deposition for sustainable textile wastewater management. *Chemical Engineering Journal*, 379: 122321.
https://doi.org/10.1016/j.cej.2019.122321

Ye WY, Liu RR, Chen XY, et al., 2020b. Loose nanofiltration-based electrodialysis for highly efficient textile wastewater treatment. *Journal of Membrane Science*, 608:118182.
https://doi.org/10.1016/j.memsci.2020.118182

Ye WY, Yu F, Yu ZJ, et al., 2024. High-performance antibacterial tight ultrafiltration membrane constructed by co-deposition of dopamine and tobramycin for sustainable high-salinity textile wastewater management. *Desalination*, 579:117482.
https://doi.org/10.1016/j.desal.2024.117482

Zhang QY, Wang X, Chen HB, et al., 2023. Eco-friendly and magnetic sucrose-derived Fe-containing mesoporous carbon composites for high-efficiency Congo red adsorption and supercapacitor applications. *Diamond and Related Materials*, 139:110268.
https://doi.org/10.1016/j.diamond.2023.110268

Zhang YB, Zhang L, Wang NN, et al., 2023. Citric acid modified β-cyclodextrin for the synthesis of water-stable and recoverable CD-MOF with enhanced adsorption sites: efficient removal of Congo red and copper ions from wastewater. *Journal of Environmental Chemical Engineering*, 11(6):111413.
https://doi.org/10.1016/j.jece.2023.111413

Electronic supplementary materials

Tables S1 and S2, Figs. S1–S10